Frequency bins for quantum information processing

Joseph M. Lukens

Research Scientist & Wigner Fellow

Quantum Information Science Group
Computational Sciences & Engineering Division
Oak Ridge National Laboratory

January 25, 2019

Time-frequency QIP

- Several QIP protocols explored, distinguished by
  - **Encoding:** discrete/continuous.
  - **Photonic mode:** time-bin/frequency-bin/pulsed.
  - **Processing:** Nonlinear mixing/linear optics.

Quantum Pulse Gate

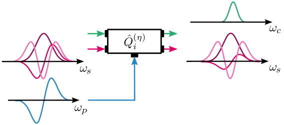

B. Brecht *et al.*, Phys. Rev. X **5**, 041017 (2015).

LOQC: *Linear-optical quantum computation*

Knill, Laflamme, & Milburn, Nature **409**, 46 (2001).

Frequency-Bin CV Cluster States

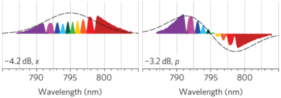

J. Roslund *et al.*, Nat. Photon. **8**, 109 (2014).

Time-Bin LOQC

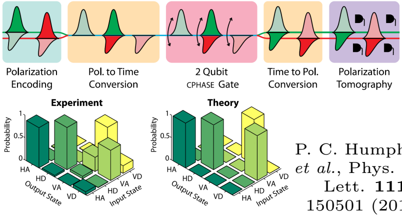

P. C. Humphreys *et al.*, Phys. Rev. Lett. **111**, 150501 (2013).

Spectral LOQC

The first discrete, linear-optical QIP protocol for frequency-bin qubits.

Why frequency bins?

- Quantum information encoded in photon frequency/wavelength.
  1. Compatible with classical telecom.
  2. Relies on optical fiber.
  3. Applicable to on-chip quantum light sources.
  4. Useful for connecting qubits in *quantum internet*.

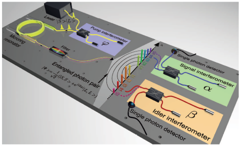

C. Reimer *et al.*, Science **351**, 1176 (2016).

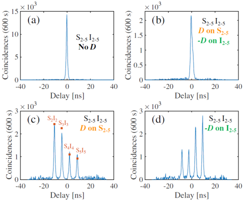

J. A. Jaramillo-Villegas *et al.*, Optica **4**, 655 (2017).

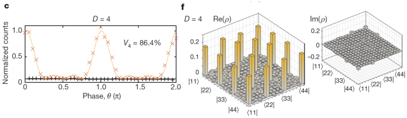

M. Kues *et al.*, Nature **549**, 622 (2017).

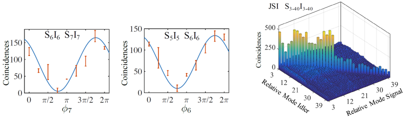

P. Imany *et al.*, Opt. Express **26**, 1825 (2018).

Why frequency bins?

- Quantum information encoded in photon frequency/wavelength.
  1. Compatible with classical telecom.
  2. Relies on optical fiber.
  3. Applicable to on-chip quantum light sources.
  4. Useful for connecting qubits in *quantum internet*.

H. J. Kimble, Nature **453**, 1023 (2008).

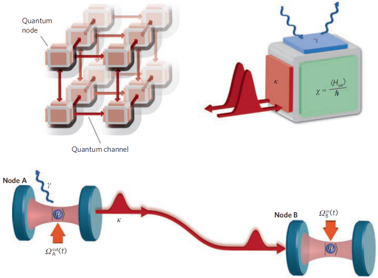

Standard Approach:
must have $\omega_A=\omega_B$

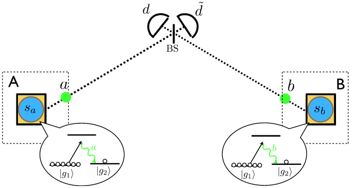

N. Sangouard *et al.*, Rev. Mod. Phys. **83**, 33 (2011).

Our Idea:
use $\omega_A \neq \omega_B$ for encoding

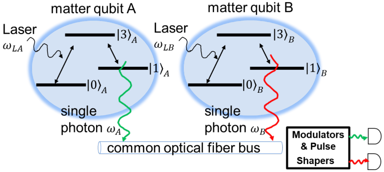

Key technology 1: Fourier-transform pulse shaping

Pulse Doublet

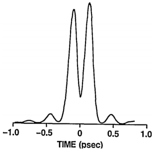

A. M. Weiner, J. P. Heritage, & E. M. Kirschner, J. Opt. Soc. Am. B **5**, 1563 (1988).

CLASSICAL EXAMPLES

4f Pulse Shaper

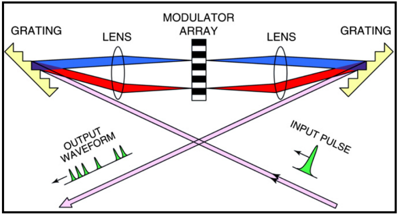

Dispersion Compensation

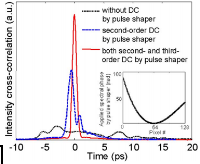

Z. Jiang *et al.*, Opt. Lett. **30**, 1449 (2005).

Comb-less Pulse Train

A. M. Weiner & D. E. Leaird, Opt. Lett. **15**, 51 (1990).

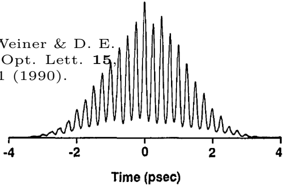

Frequency Encoding

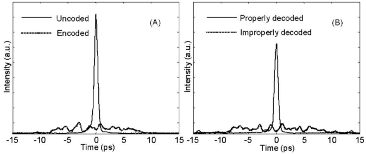

A. M. Weiner, Z. Jiang, & D. E. Leaird, J. Opt. Netw. **6**, 728 (2007).

Key technology 1: Fourier-transform pulse shaping

Pulse Doublet

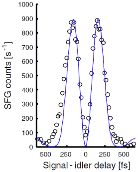

A. Pe'er *et al.*, Phys. Rev. Lett. **94**, 073601 (2005).

QUANTUM EXAMPLES

4f Pulse Shaper

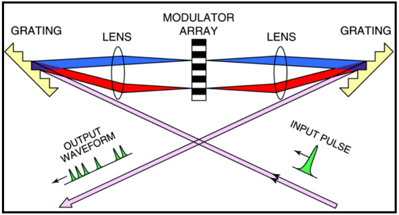

Dispersion Compensation

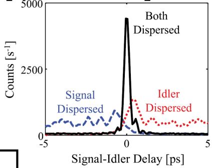

J. M. Lukens *et al.*, Phys. Rev. Lett. **111**, 193603 (2013).

Comb-less Pulse Train

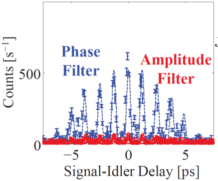

J. M. Lukens *et al.*, Opt. Express **22**, 9585 (2014).

Frequency Encoding

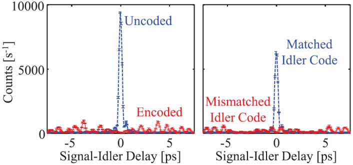

J. M. Lukens *et al.*, Phys. Rev. Lett. **112**, 133602 (2014).

Key technology 2: electro-optic modulation

Modulation Cancellation

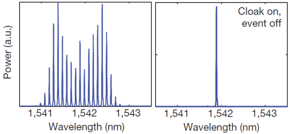

J. M. Lukens, D. E. Leaird, & A. M. Weiner, Nature **498**, 205 (2013).

CLASSICAL EXAMPLES

Tunable Delay

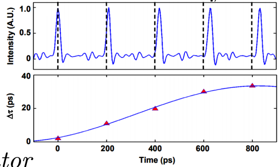

J. van Howe & C. Xu, Opt. Express **13**, 1138 (2005).

Eletro-Optic Phase Modulator

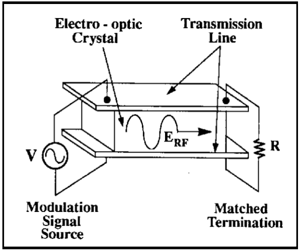

T. A. Maldonado, in *Handbook of Optics* (McGraw-Hill, 1995).

Spread Spectrum

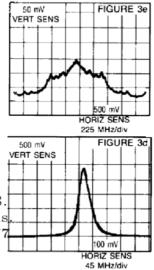

G. Vannucci & S. Yang, IEEE Trans. Commun. **37**, 777 (1989).

Time Lens

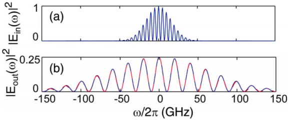

V. Torres-Company, J. Lancis, & P. Andrés, Opt. Lett. **32**, 2849 (2007).

Key technology 2: electro-optic modulation

Modulation Cancellation

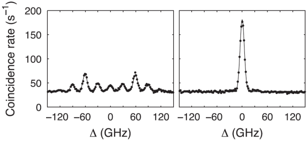

S. Sensarn, G. Y. Gin, & S. E. Harris, Phys. Rev. Lett. **103**, 163601 (2009).

QUANTUM EXAMPLES

Tunable Delay

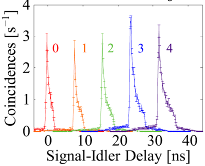

O. D. Odele *et al.*, APL Photon. **2**, 011301 (2017).

Eletro-Optic Phase Modulator

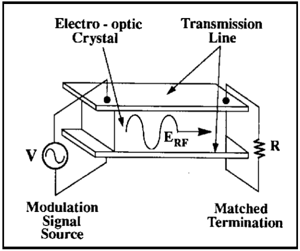

T. A. Maldonado, in *Handbook of Optics* (McGraw-Hill, 1995).

Spread Spectrum

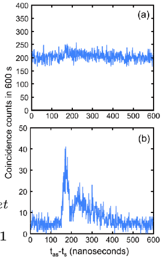

C. Belthangady *et al.*, Phys. Rev. Lett. **104**, 223601 (2010).

Time Lens

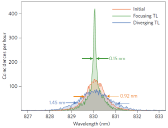

M. Karpiński *et al.*, Nat. Photon. **11**, 53 (2017).

Universal QIP with frequency-bin qubits

1. **Qubit**: One photon, two spectral bins.

$$|\psi\rangle = \alpha|0\rangle_L + \beta|1\rangle_L$$
$$= (\alpha\hat{a}_0^\dagger + \beta\hat{a}_1^\dagger)|\text{vac}\rangle$$

2. **Phase shifter**: Fourier-transform pulse shaper.

Output Mode → $\hat{b}_n = e^{i\phi_n}\hat{a}_n$ ← *Input Mode*

3. **Mode mixer**: Electro-optic phase modulator (EOM).

$$e^{i\varphi(t)} = \sum_k c_k e^{-ik\Delta\omega t}$$

Output Mode → $\hat{b}_n = \sum_k c_{n-k}\hat{a}_k$ ← *Input Mode*

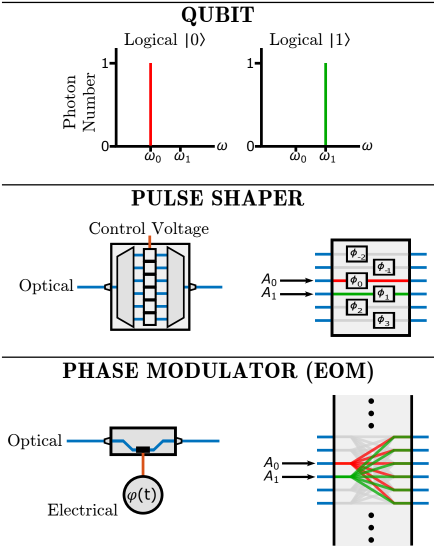

Universal QIP with frequency-bin qubits

1. **Qubit**: One photon, two spectral bins.

$$|\psi\rangle = \alpha|0\rangle_L + \beta|1\rangle_L$$
$$= (\alpha\hat{a}_0^\dagger + \beta\hat{a}_1^\dagger)|\mathrm{vac}\rangle$$

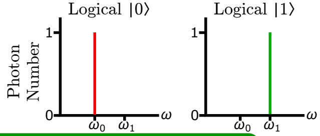

2. **Phase shi**… transform …

Output Mode → $\hat{b}_n$ …

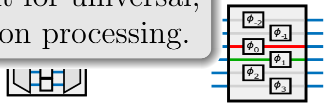

Our Findings

These elements are sufficient for universal, scalable quantum information processing.

3. **Mode mixer**: Electro-optic phase modulator (EOM).

$$e^{i\varphi(t)} \quad \sum \quad e^{-ik\Delta\omega t}$$

Output Mode → $\hat{b}_n = \sum_k c_{n-k}\hat{a}_k$ … *Mode*

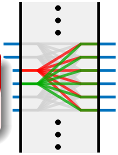

Theory Paper

J. M. Lukens & P. Lougovski, *Optica* **4**, 8–16 (2017).

Quantum frequency processor (QFP)

- Our experiments so far have concentrated on a quantum frequency processor (QFP) with

  i. *Three elements (EOM–PS–EOM).*

  ii. *Sinewave-only EO modulation.*

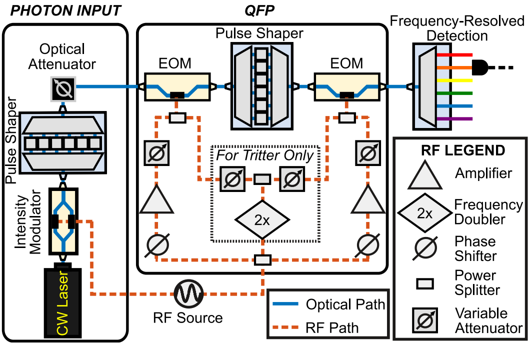

Basic QFP

- Enables near-ideal single-qubit gates, and high-fidelity two-qubit gates.
- Characterize with classical frequency comb, using method analogous to [S. Rahimi-Keshari *et al.*, Opt. Express **21**, 13450 (2013)].

Quantum frequency processor (QFP)

- Our experiments so far have concentrated on a quantum frequency processor (QFP) with

  i. *Three elements (EOM–PS–EOM).*

  ii. *Sinewave-only EO modulation.*

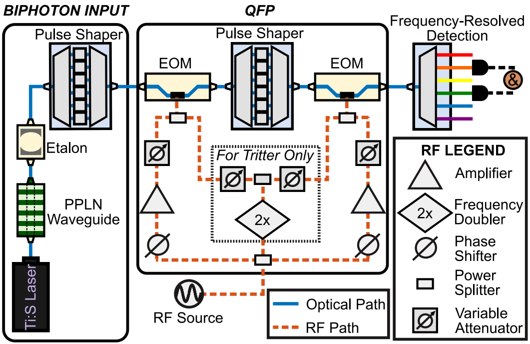

Basic QFP

- Enables near-ideal single-qubit gates, and high-fidelity two-qubit gates.
- Characterize with classical frequency comb, using method analogous to [S. Rahimi-Keshari *et al.*, Opt. Express **21**, 13450 (2013)].

Experimental setup at Oak Ridge

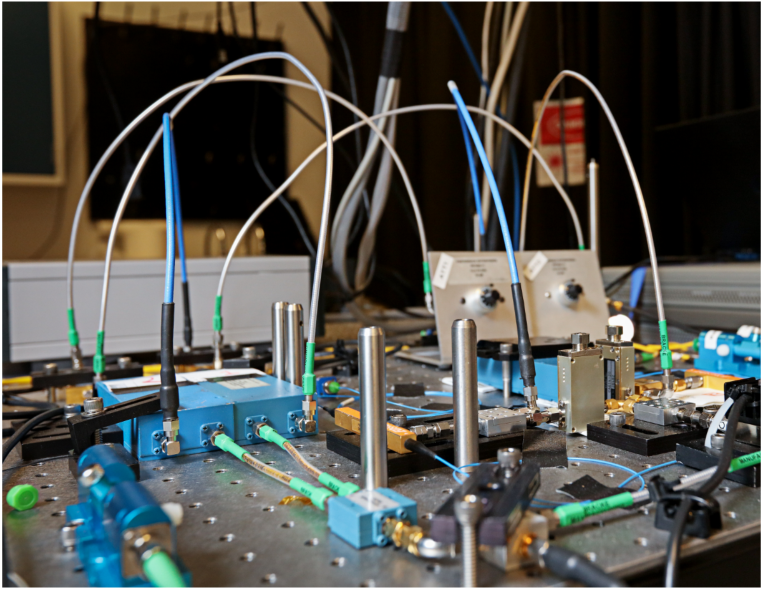

Experimental setup at Oak Ridge

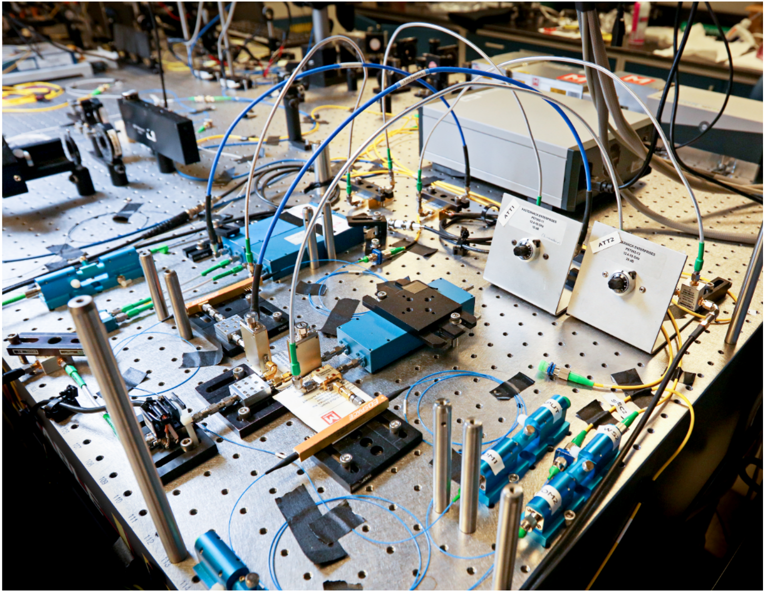

Experimental setup at Oak Ridge

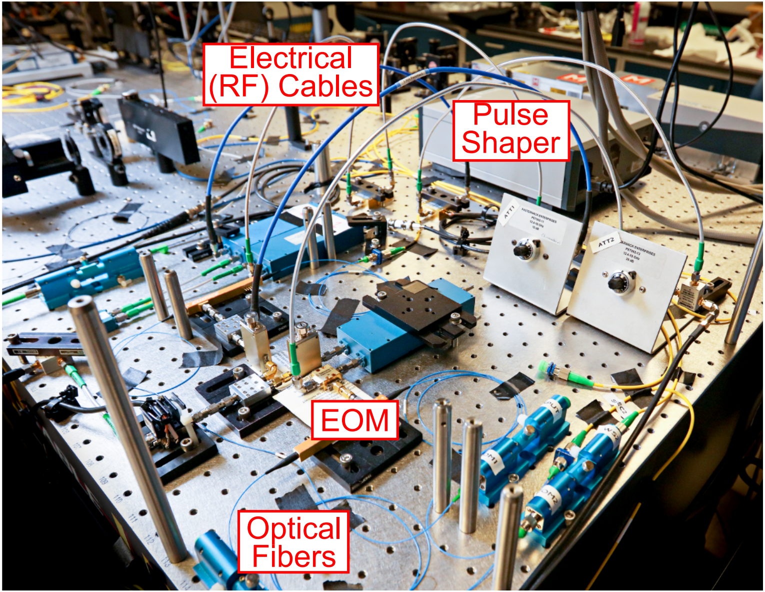

Frequency beamsplitter

- Implemented the frequency-bin beamsplitter (Hadamard H gate) experimentally.
- Measured $\boxed{\mathcal{F} = 0.99998 \pm 0.00003}$ & $\boxed{\mathcal{P} = 0.9739 \pm 0.0003}$. Examples:

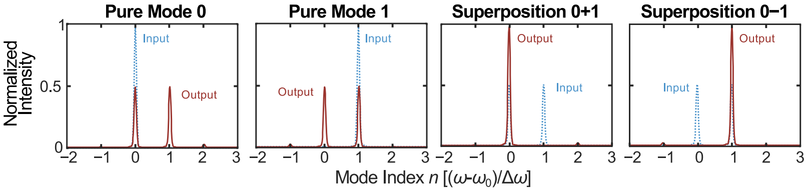

Frequency beamsplitter

- Implemented the frequency-bin beamsplitter (Hadamard H gate) experimentally.
- Measured $\boxed{\mathcal{F} = 0.99998 \pm 0.00003}$ & $\boxed{\mathcal{P} = 0.9739 \pm 0.0003}$. Examples:

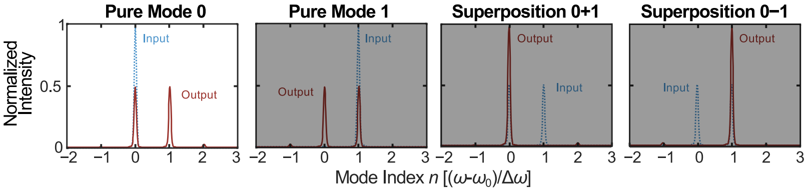

Frequency beamsplitter

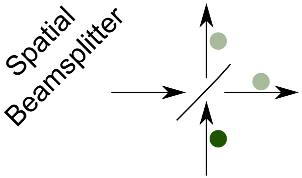

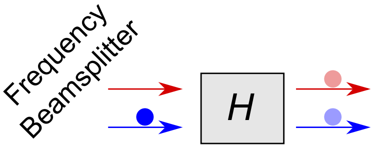

- Implemented the frequency-bin beamsplitter (Hadamard H gate) experimentally.
- Measured $\boxed{\mathcal{F} = 0.99998 \pm 0.00003}$ & $\boxed{\mathcal{P} = 0.9739 \pm 0.0003}$. Examples:

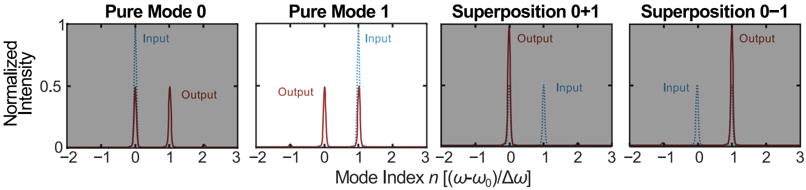

Frequency beamsplitter

- Implemented the frequency-bin beamsplitter (Hadamard H gate) experimentally.
- Measured $\boxed{\mathcal{F} = 0.99998 \pm 0.00003}$ & $\boxed{\mathcal{P} = 0.9739 \pm 0.0003}$. Examples:

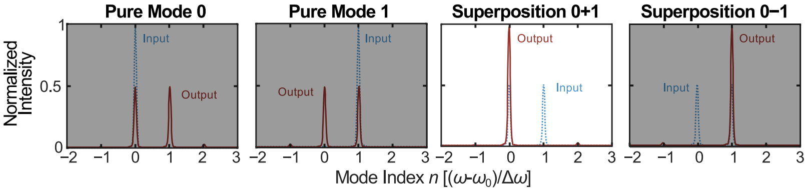

Frequency beamsplitter

- Implemented the frequency-bin beamsplitter (Hadamard H gate) experimentally.
- Measured $\boxed{\mathcal{F} = 0.99998 \pm 0.00003}$ & $\boxed{\mathcal{P} = 0.9739 \pm 0.0003}$. Examples:

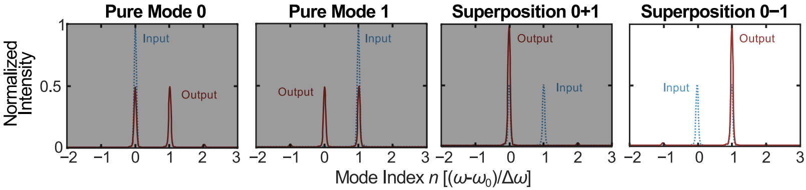

Frequency-bin tritter

- Can also extend to 3×3 system—a tritter.

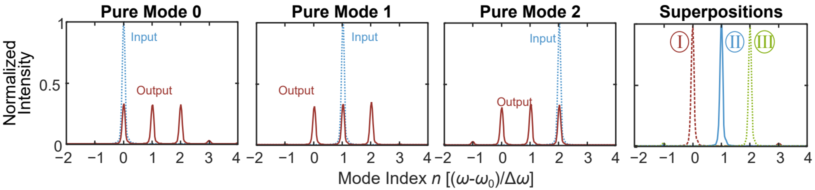

- To the single-photon level!

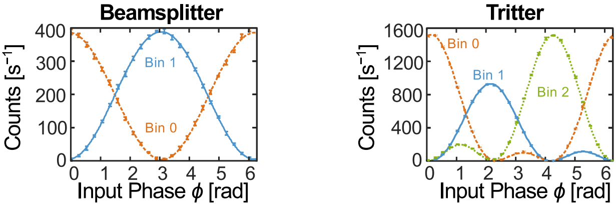

H.-H. Lu, J. M. Lukens, N. A. Peters, O. D. Odele, D. E. Leaird, A. M. Weiner, & P. Lougovski, *Phys. Rev. Lett.* **120**, 030502 (2018).

Frequency-domain Hong–Ou–Mandel interference

- Requires:
  1. Frequency beamsplitter.
  2. Tunable "distinguishability" parameter.
- Previous examples:

Basic Concept of Frequency-Domain HOM

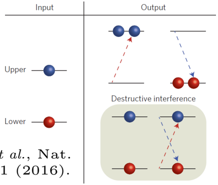

T. Kobayashi *et al.*, Nat. Photon. **10**, 441 (2016).

$\chi^{(2)}$ mixer, scan delay

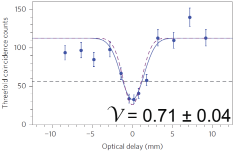

T. Kobayashi *et al.*, Nat. Photon. **10**, 441 (2016).

$\chi^{(3)}$ mixer, scan frequency spacing

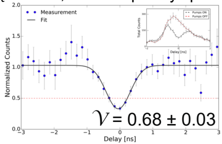

C. Joshi, A. Farsi, & A. Gaeta, CLEO **FF2E.3** (2017).

EO mixer, scan frequency spacing

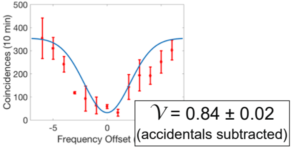

P. Imany, O. D. Odele, M. S. Al Alshaykh, H.-H. Lu, D. E. Leaird, & A. M. Weiner, Opt. Lett. **43**, 2760 (2018).

Our approach

We tune BS reflectivity $\mathcal{R}$ by scanning pulse shaper phase shift α.

Our frequency-bin HOM interferometer

- Filter out central modes: $|\Psi\rangle = |\omega_0\rangle_A |\omega_1\rangle_B$.
- Scan α for tunable BS between ω_0 and ω_1.
- Coincidences: $C_{01} \propto |\mathcal{R}(\alpha) - \mathcal{T}(\alpha)|^2$.

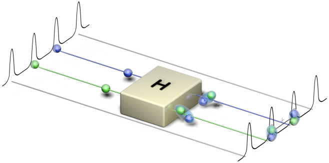

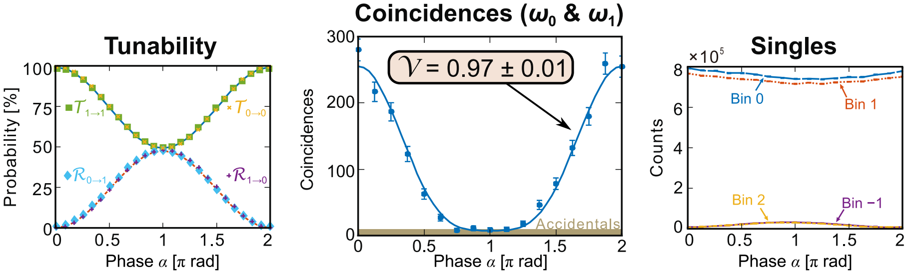

Findings

1. Record-high visibility for frequency HOM: $\mathcal{V} = 0.97 \pm 0.01$.
2. Minimal scattering to adjacent modes.

Our frequency-bin HOM interferometer

- Filter out central modes: $|\Psi\rangle = |\omega_0\rangle_A |\omega_1\rangle_B$.
- Scan α for tunable BS between ω_0 and ω_1.
- Coincidences: $C_{01} \propto |\mathcal{R}(\alpha) - \mathcal{T}(\alpha)|^2$.

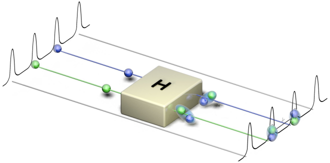

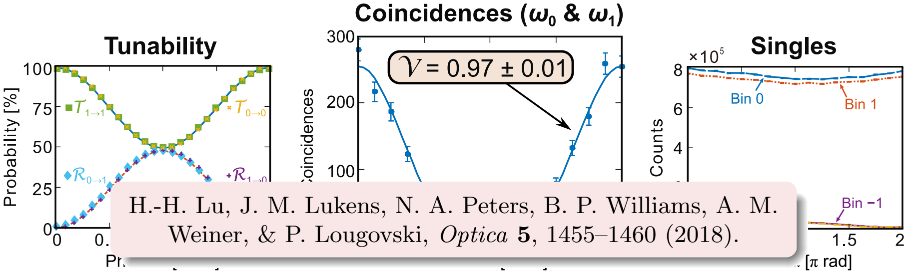

H.-H. Lu, J. M. Lukens, N. A. Peters, B. P. Williams, A. M. Weiner, & P. Lougovski, *Optica* **5**, 1455–1460 (2018).

Findings

1. Record-high visibility for frequency HOM: $\mathcal{V} = 0.97 \pm 0.01$.
2. Minimal scattering to adjacent modes.

Multi-qubit control

- New aspects demonstrated by our HOM interferometer:
  1. *Tunable reflectivity* $\Rightarrow$ reconfigurable quantum gates.
  2. *Frequency-based tuning* $\Rightarrow$ independent gates in parallel in **same configuration**.

Operation on two qubits

We set up two single-qubit gates in parallel, each is either identity $\mathbb{1}$ ($\mathcal{R} = 0$) or Hadamard H ($\mathcal{R} = 0.5$).

- Filtered input: $|\Psi\rangle = |\omega_{-4}\rangle_A |\omega_5\rangle_B + |\omega_{-3}\rangle_A |\omega_4\rangle_B$

$$\mathbb{1}_A \otimes \mathbb{1}_B \longrightarrow |\omega_{-4}\rangle_A |\omega_5\rangle_B + |\omega_{-3}\rangle_A |\omega_4\rangle_B$$

$$H_A \otimes \mathbb{1}_B \longrightarrow |\omega_{-4}\rangle_A |\omega_4\rangle_B + |\omega_{-4}\rangle_A |\omega_5\rangle_B - |\omega_{-3}\rangle_A |\omega_4\rangle_B + |\omega_{-3}\rangle_A |\omega_5\rangle_B$$

$$\mathbb{1}_A \otimes H_B \longrightarrow |\omega_{-4}\rangle_A |\omega_3\rangle_B - |\omega_{-4}\rangle_A |\omega_5\rangle_B + |\omega_{-3}\rangle_A |\omega_4\rangle_B + |\omega_{-3}\rangle_A |\omega_5\rangle_B$$

$$H_A \otimes H_B \longrightarrow |\omega_{-4}\rangle_A |\omega_4\rangle_B + |\omega_{-3}\rangle_A |\omega_5\rangle_B$$

Multi-qubit control

- New aspects demonstrated by our HOM interferometer:
  1. *Tunable reflectivity* ⇒ reconfigurable quantum gates.
  2. *Frequency-based tuning* ⇒ independent gates in parallel in **same configuration**.

Operation on two qubits

We set up two single-qubit gates in parallel, each is either identity $\mathbb{1}$ ($\mathcal{R} = 0$) or Hadamard H ($\mathcal{R} = 0.5$).

- Filtered input: $|\Psi\rangle = |\omega_{-4}\rangle_A |\omega_5\rangle_B + |\omega_{-3}\rangle_A |\omega_4\rangle_B$

$\mathbb{1}_A \otimes \mathbb{1}_B \longrightarrow |\omega$

Negative frequency correlations

$H_A \otimes \mathbb{1}_B \longrightarrow | \ldots \omega_4\rangle_B + |\omega_{-3}\rangle_A |\omega_5\rangle_B$

No frequency correlations

$\mathbb{1}_A \otimes H_B \longrightarrow |\omega \ldots \omega_4\rangle_B + |\omega_{-3}\rangle_A |\omega_5\rangle_B$

$H_A \otimes H_B \longrightarrow |$

Positive frequency correlations

Independent, parallel qubit control

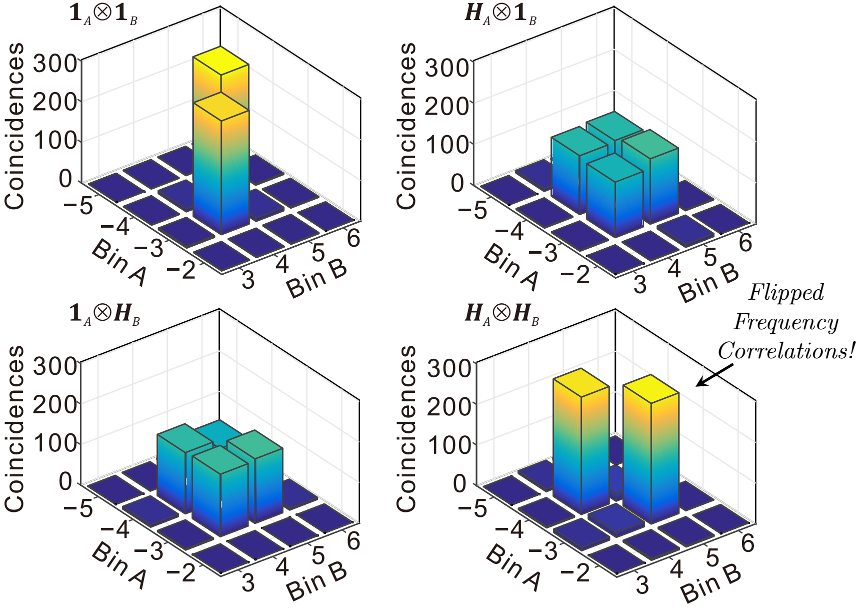

Independent, parallel qubit control

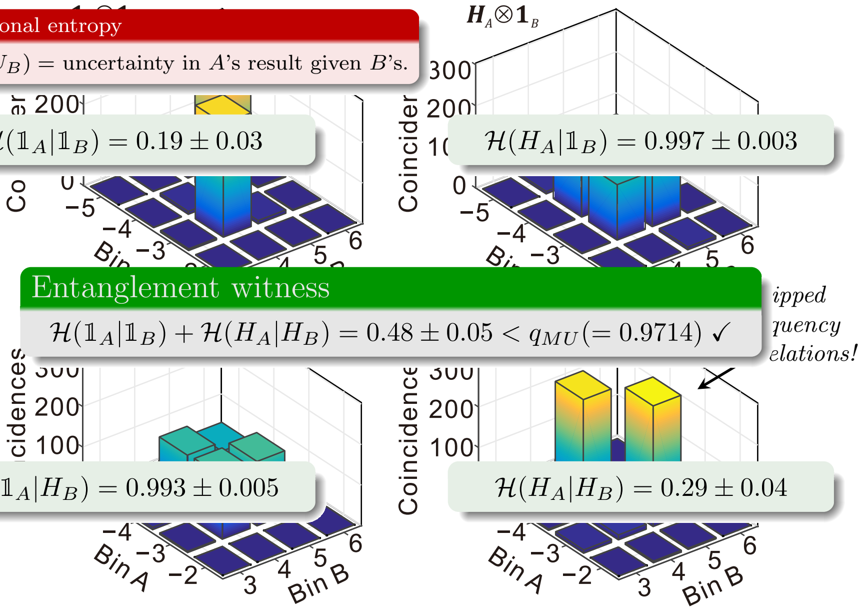

Conditional entropy

$\mathcal{H}(U_A|U_B)$ = uncertainty in A's result given B's.

$\mathcal{H}(\mathbb{1}_A|\mathbb{1}_B) = 0.19 \pm 0.03$

$\mathcal{H}(H_A|\mathbb{1}_B) = 0.997 \pm 0.003$

Entanglement witness

$\mathcal{H}(\mathbb{1}_A|\mathbb{1}_B) + \mathcal{H}(H_A|H_B) = 0.48 \pm 0.05 < q_{MU} (= 0.9714)$ ✓

$\mathcal{H}(\mathbb{1}_A|H_B) = 0.993 \pm 0.005$

$\mathcal{H}(H_A|H_B) = 0.29 \pm 0.04$

Bayesian state reconstruction

- BME can recover full state from previous four measurements alone.
- Retrieved error accounts for missing information.

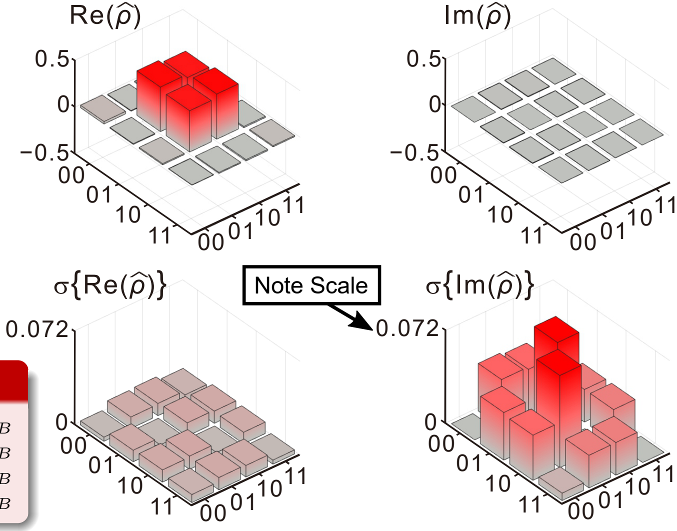

Legend

$00 \equiv |1_{\omega_{-4}}\rangle_A |1_{\omega_4}\rangle_B$
$01 \equiv |1_{\omega_{-4}}\rangle_A |1_{\omega_5}\rangle_B$
$10 \equiv |1_{\omega_{-3}}\rangle_A |1_{\omega_4}\rangle_B$
$11 \equiv |1_{\omega_{-3}}\rangle_A |1_{\omega_5}\rangle_B$

Bayesian state reconstruction

- BME can recover full state from previous four measurements alone.
- Retrieved error accounts for missing information.

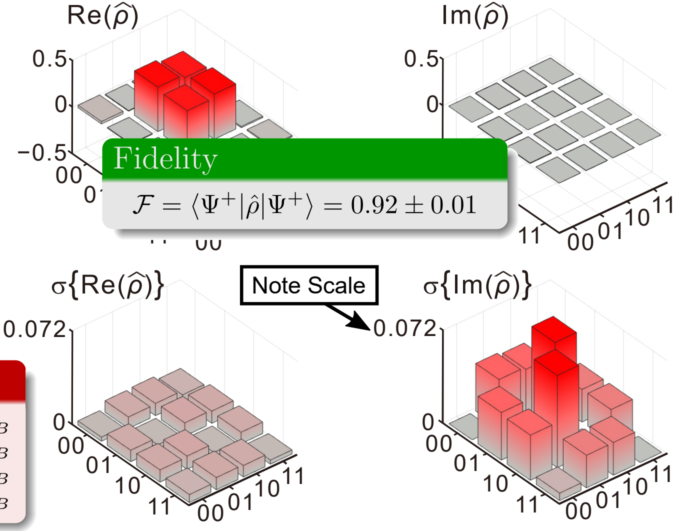

Fidelity

$$\mathcal{F} = \langle \Psi^+ | \hat{\rho} | \Psi^+ \rangle = 0.92 \pm 0.01$$

Legend

$00 \equiv |1_{\omega_{-4}}\rangle_A |1_{\omega_4}\rangle_B$

$01 \equiv |1_{\omega_{-4}}\rangle_A |1_{\omega_5}\rangle_B$

$10 \equiv |1_{\omega_{-3}}\rangle_A |1_{\omega_4}\rangle_B$

$11 \equiv |1_{\omega_{-3}}\rangle_A |1_{\omega_5}\rangle_B$

Two-qubit gate

- Entangling gates also necessary for universal QIP.
- Challenging with optics, but possible probabilistically.
- Design and implement coincidence-basis CNOT in our QFP.

CONTROL/TARGET BIN DEFINITIONS

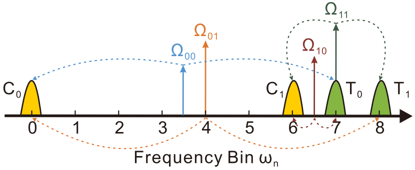

CLASSICAL CHARACTERIZATION

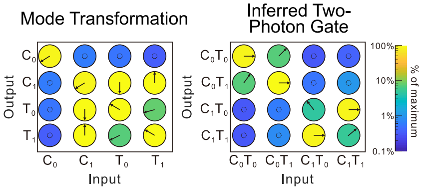

QUANTUM TESTS

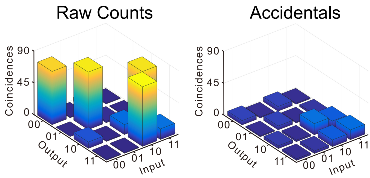

Key result

First entangling gate for frequency-encoded qubits, in any platform.

Two-qubit gate

- Entangling gates also necessary for universal QIP.
- Challenging with optics, but possible probabilistically.
- Design and implement coincidence-basis CNOT in our QFP.

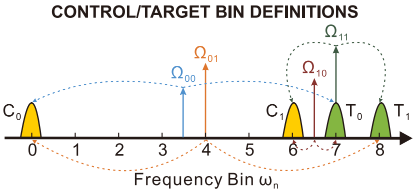

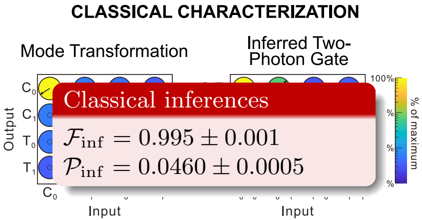

Classical inferences

$\mathcal{F}_{\text{inf}} = 0.995 \pm 0.001$

$\mathcal{P}_{\text{inf}} = 0.0460 \pm 0.0005$

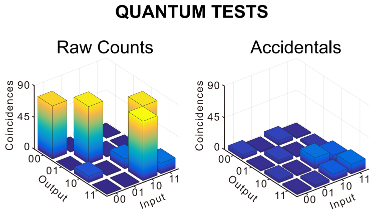

Key result

First entangling gate for frequency-encoded qubits, in any platform.

Back to Bayes

- Conventional reconstruction provides no information on coherence from computational basis alone.
- We develop model and apply *Bayesian machine learning* and slice sampling to analyze the full quantum CNOT.
- Utilizes all data: singles, coincidences, no counts.

$$P(\mathcal{D}|\beta) = (p_A - p_{AB})^{N_A - N_{AB}} (p_B - p_{AB})^{N_B - N_{AB}} \times p_{AB}^{N_{AB}} (1 - p_A - p_B + p_{AB})^{M - N_A - N_B + N_{AB}}$$

- Obtain quantum unitary fidelity of $\boxed{\mathcal{F}_{\text{Bayes}} = 0.91 \pm 0.01}$.

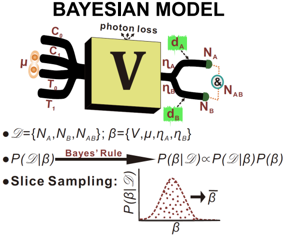

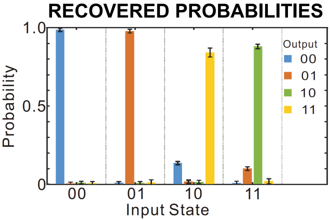

Bayesian machine learning

Extracts details from experimental data hidden from traditional quantum characterization methods.

Back to Bayes

- Conventional reconstruction provides no information on coherence from computational basis alone.
- We develop model and apply *Bayesian machine learning* and slice sampling to analyze the full quantum CNOT.
- Utilizes all data: singles, coincidences, no counts.

$$P(\mathcal{D}|\beta) = (p_A - p_{AB})^{N_A - N_{AB}} (p_B - p_{AB})^{N_B - N_{AB}}$$

- Obtai

$\mathcal{F}_{\text{Bayes}}$

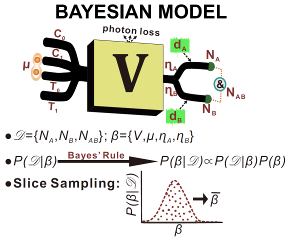

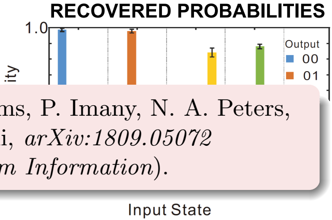

H.-H. Lu, J. M. Lukens, B. P. Williams, P. Imany, N. A. Peters, A. M. Weiner, & P. Lougovski, *arXiv:1809.05072* (to appear in *npj Quantum Information*).

Bayesian machine learning

Extracts details from experimental data hidden from traditional quantum characterization methods.

Applications for frequency-bin QIP

- Demonstrated universal gate set. What's on the horizon?
  1. Quantum simulation.
  2. Time-frequency hyperencoding.
  3. On-chip integration for scalability, low loss.
  4. Quantum node connections.
  5. Classical all-optical networking.

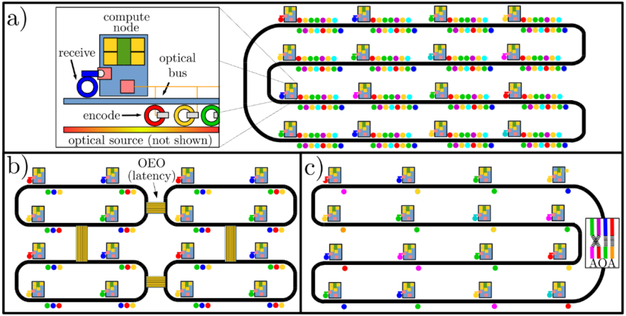

QUANTUM SIMULATION

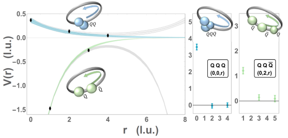

HIGH-*D* SUM GATE

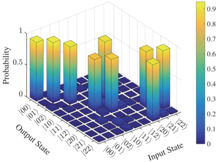

↑ **UPPER:** H.-H. Lu *et al.*, arXiv:1810.03959 (2018).

↑ **LOWER:** P. Imany *et al.*, arXiv:1805.04410 (2018).

Acknowledgments

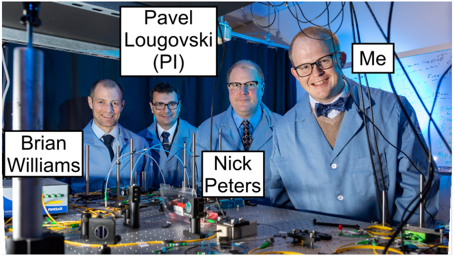

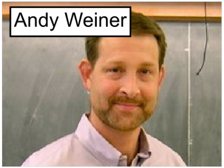

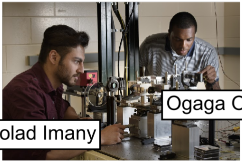

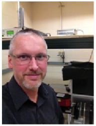

Dan Leaird

References

Optica **4**, 8–16 (2017); *Phys. Rev. Lett.* **120**, 030502 (2018); *Optica* **5**, 1455–1460 (2018); *arXiv:1809.05072* (2018).